# Marine source signature estimation with dual near-field hydrophones

*Rob Telling\*, Sergio Grion Stuart Denny & R. Gareth Williams, Shearwater GeoServices*

## Summary

We derive marine seismic signatures using twice the usual number of near-field hydrophones, following the proposition of Parkes and Hatton (1986), in which the notional sources and their virtual image are solved for directly. This removes the need to assume a value for the free-surface reflectivity and amounts to a separation of the up-going and down-going wave-field in the vicinity of the source array. A test sequence of near-field records and seismic data were acquired. Inspection of the near-field recordings revealed clipping of large negative amplitudes, probably related to cavitation in the water, explaining an observed reduction in amplitude of the ghost in the derived signature. We evaluated the signatures via processing of the seismic data and compared them against signatures derived from a single NFH per source element, using a parametric ghost model (Hargreaves *et al.*, 2016).

## Introduction

Marine source signature estimation using near-field hydrophone measurements (e.g. Ziolkowski *et al.*,1982, Parkes *et al.*, 1984) is a well-established procedure and is now recognized as important for accurate broadband de-signature of seismic data. In the case of a single NFH per source element, it is necessary to define a model for the propagation of sound from each source element (a translating and pulsating bubble of air) to each receiver, comprising phase shift and amplitude scaling terms. The precise layout of sources and receivers must be known together with the reflectivity of the sea-surface to account for direct and reflected paths (ghosts). With $n$ hydrophone measurements and $n$ notional sources to solve for, the problem is well posed. Parkes and Hatton (1986) proposed that this scheme could be extended, whereby $2n$ hydrophones are used and a series of $n$ virtual sources (in mirror positions above the sea-surface) are additionally solved for. This then removes both the need to model the ghost path, and to parameterize the sea-surface reflectivity.

Hampson (2017) and Kryvohuz and Campman (2017) recently revived interest in these ideas, separating the wave-field to better-understand the physics occurring in the vicinity of the array and to improve characterization of the source ghost in the far-field signature. Here we describe an acquisition test carried out early in 2018, where near-field hydrophone data and the associated (far-field) streamer data were recorded with the aim of evaluating the benefit of additional measurements and of the virtual notional concept in particular. We estimated reference far-field signatures first using a standard ghost model and notional source estimation, and then via joint estimation of source and virtual source notionals, finally evaluating the results with a de-signature processing sequence.

## Near-field recordings

The test source array comprised two strings each with six source elements (either an air-gun or air-gun cluster) nominally at 7m depth, spaced at 3m in-line, with 8m cross-line between the strings. Total volume for the two strings was 2740in$^3$. Near-field hydrophones were used to instrument the array at depths of 6m and 4m as in Figure 1. The shallower hydrophones were attached to the vertical suspension for the test, which led to some additional noise on the recordings; however for the main events the signal-to-noise was high.
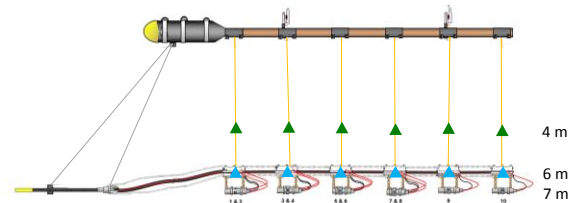


Figure 1: Schematic layout of the source string showing the standard position of hydrophones 1m above guns (blue triangles) and additional hydrophones at 3m above guns (green triangles), attached to ropes.
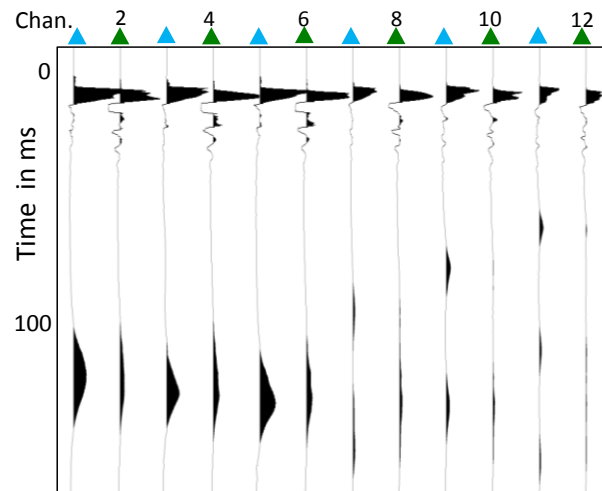


Figure 2: Example near-field hydrophone recordings from the starboard string at the standard positions 1m above the gun ports (odd channels, blue triangles) and in the test position at 3m above the gun ports (even channels, green triangles). Adjacent traces are co-located in x and y.

An example of the recordings, sampled at 0.5ms, is given in Figure 2. A feature in the shallower recordings (which are closer to the sea-surface so that the ghost features more prominently) is that when the positive pulse is large, the negative amplitude is clipped. After this, there follow some additional oscillations. The same ghost-related events also appear in the deeper recording but at much reduced amplitude relative to the more prominent positive arrivals.
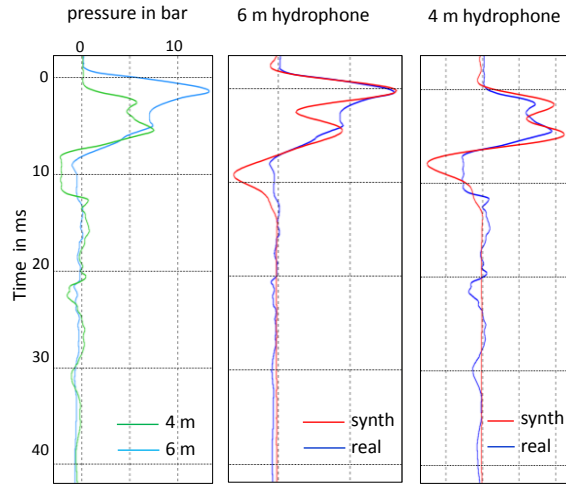


Figure 3: Real NFH recordings for channels 1 and 2 (left) and comparison between real and synthetic recordings (centre and right), co-located in x-y at depths of 4m and 6m from the fore end of the starboard string.

As an exercise to understand the event timing and amplitudes in the recorded traces better, we created synthetics by forward modelling a simple Ormsby wavelet defined by four frequencies *viz.* 1-4-100-400Hz. In the synthetics, we assumed a ghost model with standard assumptions about the reflectivity arising from a 1m significant wave height rough sea-surface (see for example Jovanovich *et al.,* 1983), consistent with the sea state as described in the observer logs. Synthetic and real traces are compared in Figure 3 (centre and right) for a position at one end of a string and in Figure 4 for a position near the centre of a string. There is broad agreement on the timing, peak levels and shape of the positive arrivals but much poorer agreement on the ghost arrivals, notably due to clipped amplitudes and the appearance of subsequent lower-amplitude oscillations at about 10ms intervals. When the positive pulse is sufficiently large, of magnitude several bar, the reflection at a free-surface is expected to form a ghost of comparable amplitude and opposite sign. However, as this ghost develops, so the pressure will drop below zero. For example at 5m depth, the water would be expected to be under tension beyond -1.5bar. Hence the

ghost pulse will tend to cause transient cavitation e.g. as described in Landro *et al.* (2016) and ultimately the wavelet is clipped.

**Signature estimation and processing**

We estimated reference signatures using a least squares inversion method (Hargreaves *et al.* 2015, 2016) deriving 12 notional sources using recordings from just the 12 hydrophones placed at 1m from the guns (method 1) and then we also estimated signatures using the full set of 24 hydrophones (Parkes and Hatton, 1986, Hampson, 2017) to derive 12 notional sources and 12 image sources (method 2). In method 2, the primary and ghost components of the far-field may be separately constructed from the corresponding set of derived notional signatures – see Figure 5 (top image) or combined to give the total estimated far-field signature including the ghost – see Figure 5 (lower image). We used measured x, y and z coordinates of each source element derived from R-GPS positions and gun depth sensors respectively and assumed mirror positions for the virtual source element positions.
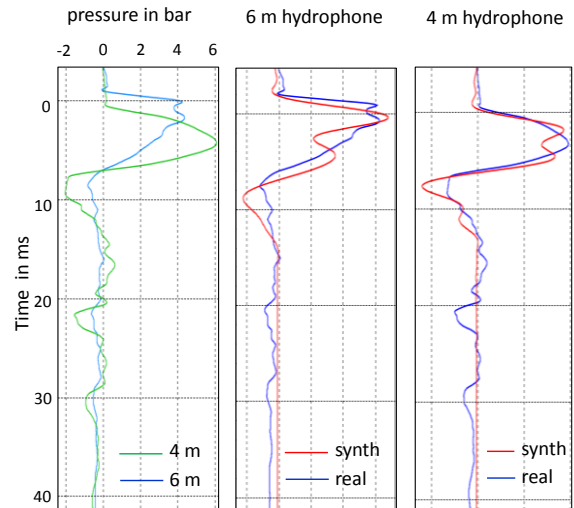


Figure 4: Real NFH recordings for channels 7 and 8 (left) and comparison between real and synthetic recordings (centre and right), co-located in x-y at depths of 4m and 6m, located 9m inline (near the centre) along the starboard string.

The smaller ghost and additional events after the ghost that were seen in the near-field recordings are also apparent in the far-fields. The comparison between the total signature derived using dual NFHs without a free-surface assumption (method 2) and the reference signature derived using single NFHs and a free-surface reflectivity defined by a significant wave height parameter (method 1) are shown in Figure 6. The upper image was derived using h=1m and the

lower figure using h=4m (see Telling *et al.* 2018 for more detail). For reference, in the vicinity of the ghost notch frequency (nominally 107 Hz) for *h*=1m we have a reflection coefficient, **r** =-0.97 and for *h*=4m, we have **r** =-0.65. In both cases we have r =-1.0 at 0Hz.
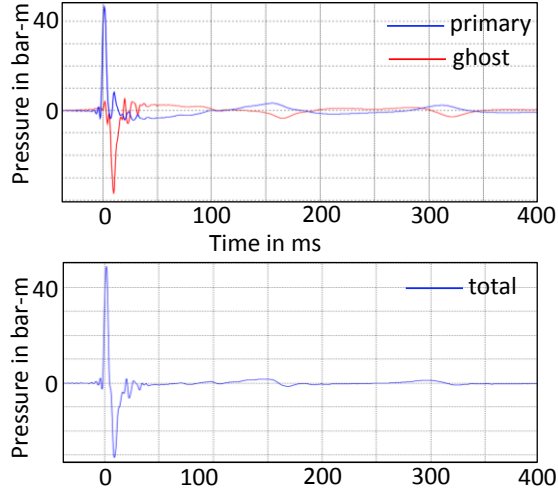


Figure 5: The top image shows far-field signatures at vertical take-off estimated by method 2. Source notional signatures labeled primary (blue), and image source notional signatures labeled ghost, (red). The lower image shows the far-field signature derived from both source and image source notional signatures (labeled total).
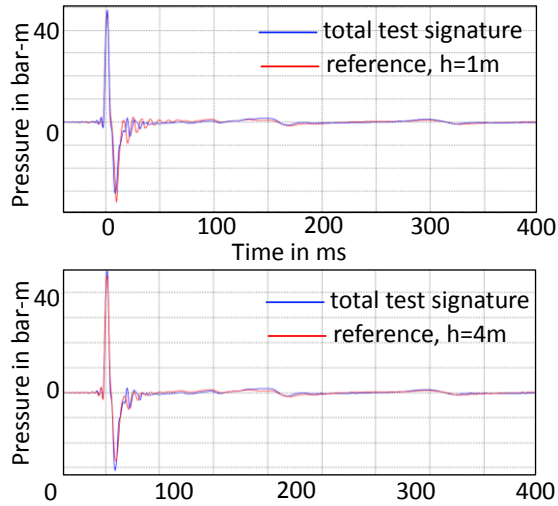


Figure 6: The top image shows the vertical-take-off far-field signature estimated by method 2 using real and image notional signatures (labeled total, in blue) compared against a signature estimated using method 1 (labeled reference, in red) with the assumption of a wave height parameter, *h*=1m (top image) and *h*=4m (lower image).

The corresponding spectra for the signatures are shown in in Figure 7 for the two different assumptions on sea-surface reflectivity. The spectrum for the reference signature, derived assuming the larger wave height parameter *h*=4m (reduced reflection coefficient at high frequency) is a closer approximation to the test signature but not identical.

Directional signatures were derived for methods 1 and 2 from -30 to +70 degrees, and a de-signature operation applied to the seismic data in tau-p, encapsulating source de-ghosting, de-bubble and matching to a zero-phase Ormsby wavelet. The results are shown in Figure 8 and indicate successful de-signature for all but the reference obtained from method 1 with nominal wave height parameter h=1m, which exhibits some residual ghosting artifacts. A further observation (not shown in these images, as it was only apparent at high angles e.g. far-offsets and on the direct arrival) is a slightly poorer performance for the test signature at de-convolving the later time bubble pulses. We noted higher noise level for the NFHs mounted at the 4m position: the relatively small bubble signal at later times means a lower signal-to-noise, which could explain this performance deficit. A dedicated rigid mounting position for these NFHs would help in this regard.
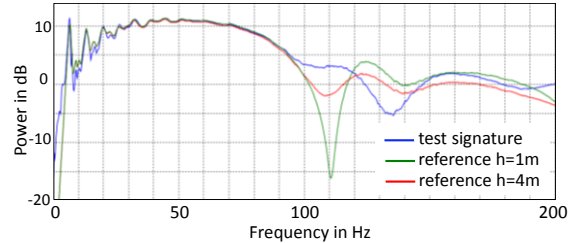


Figure 7: Spectra for vertical-take-off far-field signature estimated by method 2 (labeled test signature, blue) compared with signature estimated using method 1 (labeled reference) with assumed wave height parameter, *h*=1m (green curve) and *h*=4m (red curve).

**Conclusions**

Using additional NFH measurements of a two-string source array, we were able to derive a series of far-field signatures without making assumptions on the free-surface reflectivity; we used the derived far-field signatures to successfully de-signature the seismic data. The quality of the signatures appears to offer an improvement over those derived via the reference method with assumed nominal sea-surface reflectivity. This is principally due to the better representation of the ghost. When the magnitude of reflectivity is reduced at high frequencies (more so than expected for the given sea-state), results of the two methods are more comparable. This independent result obtained using extra NFHs validates the use of frequency dependent reflection coefficients.
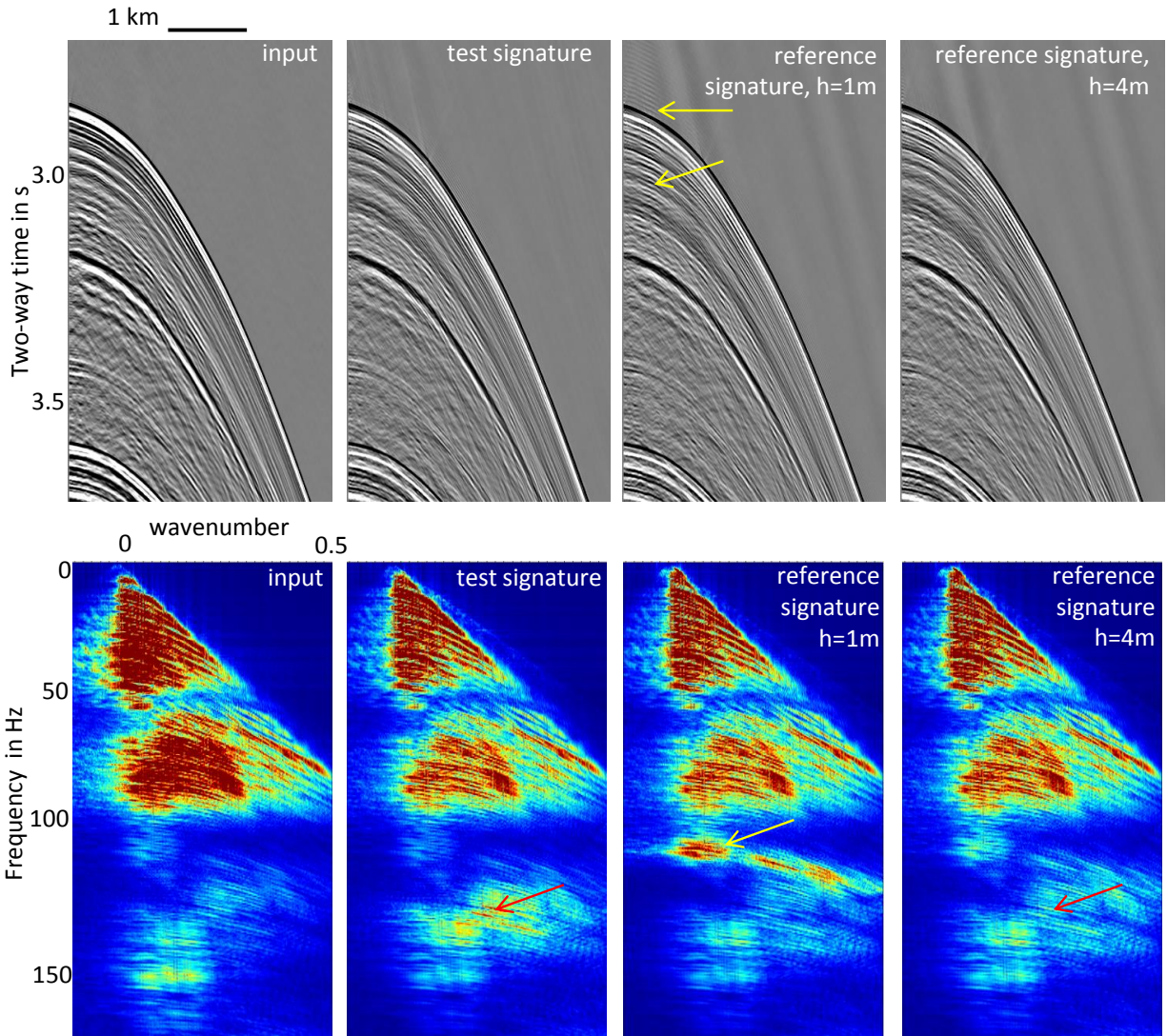
Figure 8: De-signature applied to shot gathers using the test signature of method 2 and two variants of reference signature from method 1. For the h=1m reference there is ringing in the shallow data indicated by the yellow arrows. The reference for h=4m is comparable with the result for the test signature. The lower images show corresponding *f-k* spectra (wavenumber normalized by 1/sample interval). The yellow arrow highlights artifacts from poor de-ghosting. The red arrows highlight a small difference between the two acceptable results arising from spectral differences in the signatures in the band 100-150 Hz.

The ghost amplitude is lower than expected for the given sea-state as observed here and in other studies (e.g. Ni *et al.* 2012, Telling *et al.* 2018) and this is probably explained as a result of the limit of tensile strength of water and onset of cavitation: positive pressures with several bars of magnitude are emitted from the array and reflection at a free-surface will ultimately attempt to drop the pressure below zero. Standard signature estimation from near-field recordings works well, but requires ghost parameterization and optimization. Doubling the NFH count to enable derivation of source and image source notionals is an attractive and promising alternative approach.

**Acknowledgements**

**Signature estimation with dual near-field hydrophones**

**References**

Hampson, G. [2017]. Notional ghosts. *86<sup>th</sup> Annual SEG Meeting* Expanded Abstracts

Hargreaves, N., Grion, S. and Telling, R. [2015]. Estimation of air-gun array signatures from near-gun measurements - least-squares inversion, bubble motion and error analysis. *85th SEG Meeting* Expanded Abstracts, 149-153.

Hargreaves, N., Telling, R., Grion, S. [2016]. Source deghosting and directional designature using near-field derived airgun signatures. *78th EAGE Conference and Exhibition*, Extended Abstracts

Jovanovich, D. B, Sumner, R. D. and Atkins-Easterlin, S. L. [1983]. Ghosting and marine signature deconvolution. *Geophysics*, **48** (11) 1468-1485.

Kryvohuz, M. and Campman, X. [2017]. Source-side up-down wavefield separation using dual NFHs, *79<sup>th</sup> EAGE Conference and Exhibition*, Extended Abstracts

Landro, M., Ni, Y. and Amundsen, L. [2016]. Reducing high-frequency ghost cavitation signals from marine air-gun arrays, *Geophysics,* **81**, P33-P46

Ni, Y., Niang, C., Siliqi, R. [2012]. Monitoring the stability of airgun source array signature. *82<sup>nd</sup> Annual SEG Meeting,* Expanded Abstracts, 1-5

Parkes, G. E., Ziolkowski, A., Hatton, L. and Haugland, T. [1984]. The signature of an airgun array: computation from near-field measurements including interactions — Practical considerations. *Geophysics*, **49**, 105–111

Parkes, G. and Hatton, L. [1986] *The Marine Seismic Souce*. D. Reidel, Dordrecht

Telling, R. H., Light, R., Grion, S., Denny, S. and Williams, R. G. [2018] Signature estimation and drop-out implications for a triple source marine seismic survey *80<sup>th</sup> EAGE Conference and Exhibition*, Extended Abstracts

Ziolkowski, A., Parkes, G., Hatton, L. and Haugland T. [1982]. The signature of an air gun array: Computation from near-field measurements including interactions. *Geophysics*, **47** (10), 1413-1421.